Synergistic stabilization of emulsion gel by nanoparticles and surfactant enables 3D printing of lipid-rich solid oral dosage forms

Jenny Johannesson [a,1], Malhar Manik Pathare [b,1], Mathias Johansson [c], Christel A.S. Bergström [a], Alexandra Teleki [b,*]

[a] Department of Pharmacy, Uppsala University, SE-751 23 Uppsala, Sweden
[b] Department of Pharmacy, Science for Life Laboratory, Uppsala University, SE-751 23 Uppsala, Sweden
[c] Department of Molecular Sciences, Swedish University of Agricultural Sciences (SLU), SE-750 07 Uppsala, Sweden

GRAPHICAL ABSTRACT
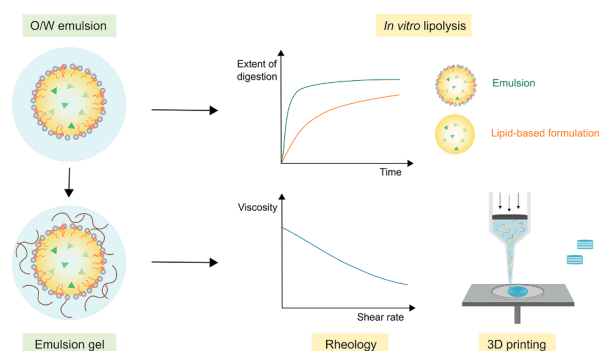
ARTICLE INFO

ABSTRACT

Pharmaceutical formulation of oral dosage forms is continuously challenged by the low solubility of new drug candidates. Pickering emulsions, emulsions stabilized with solid particles, are a promising alternative to surfactants for developing long-term stable emulsions that can be tailored for controlled release of lipophilic drugs. In this work, a non-emulsifying lipid-based formulation (LBF) loaded with fenofibrate was formulated into an oil-in-water (O/W) emulsion synergistically stabilized by stearic acid and silica (SiO_2) nanoparticles. The emulsion had a droplet size of 341 nm with SiO_2 particles partially covering the oil–water interface. *In vitro* lipid digestion was faster for the emulsion compared to the corresponding LBF due to the larger total surface area available for digestion. Cellulose biopolymers were added to the emulsion to produce a gel for semi-solid extrusion (SSE) 3D printing into tablets. The emulsion gel showed suitable rheological attributes for SSE, with a trend of higher viscosity, yield stress, and storage modulus (G′), compared to a conventional self-emulsifying lipid-based

emulsion gel. The developed emulsion gel allows for a non-emulsifying LBF to be transformed into solid dosage forms for rapid lipid digestion and drug release of a poorly water-soluble drug in the small intestine.

1. Introduction

Poor water-solubility of new drug candidates is challenging for pharmaceutical formulation and design of suitable oral drug products. Co-administration of lipids enhance the oral bioavailability of poorly water-soluble drugs. Lipid-based formulations (LBFs) are therefore a well-established formulation strategy for tackling low solubility [1–4]. These formulations are typically administered as liquid-filled gelatin capsules, where the simplest LBF, classified as LBF type I, consists of a single lipid component in which the drug is pre-dissolved. However, LBFs usually contain a mixture of oils, surfactants, and co-solvents, LBF types II–IV. Such LBFs self-emulsify upon dispersion in gastrointestinal fluids, generating a high surface area of oil droplets, which is advantageous for a rapid and uniform absorption [5–8]. Despite the ability of these formulations to enhance drug absorption of lipophilic drugs their conversion into commercial drug products is limited by several factors including high manufacturing cost and poor physicochemical stability of liquid formulations, where many drugs are prone to chemical degradation through hydrolysis in the presence of water. Solidification of lipid liquid formulations are therefore highly desirable [9]. Furthermore, the drug loading capacity of LBFs is generally low, up to around 15% w/w [10]. For low potency drugs, i.e., drugs needed to be administered at a high dose, large amounts of excipients such as surfactants are required, which can be problematic from a safety perspective, especially in specific groups like pediatric patients [11].

As an alternative to self-emulsifying LBFs containing surfactants, stabilization of oil droplets can be achieved with solid particles, called Pickering emulsions [12–14]. Pickering emulsions are highly interesting for pharmaceutical applications, as it is possible to tailor Pickering emulsion towards its application by control and modification of particle properties. In addition, Pickering emulsions exhibit good physical stability due to high resistance towards coalescence and Ostwald ripening. Pickering emulsions can be stabilized with inorganic particles. Silica (SiO_2) nanoparticles, commonly used additives in food and pharmaceuticals, have been widely studied due to their biocompatibility and ease of modification to render them partially hydrophobic [12,15]. Furthermore, SiO_2 particles enables formulation of Pickering emulsions with submicron droplets size and can be produced in large scale. Recently, the stabilization of Pickering emulsions using organic particles derived from natural sources, e.g., cellulose and starch has gained increased interest because of their well-known biodegradability and biocompatibility properties [16]. The variety of particles that can be used, as well as the possibility of particle functionalization allow for tailoring the solid particle layer at the oil–water interface for controlled lipid digestion and hence, controlled drug release [17].

Although Pickering emulsions could be used as oral dosage forms, the manufacturing of liquid-filled capsules is generally less cost-effective compared with traditional tablet production due to their bulky handling, requiring large spaces for production and transportation. However, conventional manufacturing of solid oral dosage forms also has limitations, in particular the assumption of one size and dose fits all. In light of this, additive manufacturing, colloquially referred to as 3D printing, has rapidly emerged as a flexible manufacturing technology for production of personalized dosage forms [18]. This technology allows for the production of solid dosage forms of complex geometries, with tailored drug release according to needs, and where multiple drugs may be combined in a single tablet [19]. In semi-solid extrusion (SSE), a gel-like formulation is extruded through a nozzle in a layer-by-layer fashion under pressure, driven by a mechanical piston or pressurized air. The formulation must possess adequate rheological properties, including shear-thinning behavior to allow for smooth extrusion of the material

through a narrow nozzle without occlusion. Moreover, viscoelastic properties are essential to maintain the 3D-printed structure after deposition [20,21]. Advantages with SSE include low temperature operation, a wide choice of excipients, and the possibility of a high drug load in the produced dosage form [22]. SSE has shown promising features for pharmaceutical applications and production of personalized dosage forms with precise dosing in a clinical setting, which also fulfill pharmaceutical standards [23–25].

Despite the great interest and possibilities offered by 3D printing for pharmaceutical applications, the selection of formulations is limited and mainly focused on water-soluble drugs [26]. Recent 3D-printing approaches for tackling low-solubility drugs include amorphization using hot-melt extrusion, coupled with fused deposition modeling [27,28]. Furthermore, nanotechnology-based formulation strategies have been combined with 3D printing, making use of e.g., mesoporous carrier systems [29], nanospheres [30], and nanocrystals [31] to improve drug solubility. Self-emulsifying lipid formulations have also been used in 3D printing of solid lipid tablets incorporating poorly water-soluble drugs [32–34]. These recent approaches highlight the need to further explore more advanced formulations, needed for poorly water-soluble drugs, and their potential in 3D printing of solid oral dosage forms. This study aimed to further broaden the use of lipids in 3D printing of solid dosage forms, by developing an emulsion gel stabilized with solid particles and a surfactant for delivery of the poorly water-soluble drug fenofibrate. Here, we formulated a LBF comprised of 100% lipids into an oil-in-water (O/W) Pickering emulsion synergistically stabilized with stearic acid and SiO_2 nanoparticles. The lipid digestion behavior of the developed emulsion and the corresponding plain LBF was studied *in vitro*. The drug-loaded emulsion was formulated into an emulsion gel for SSE 3D printing into solid tablets and the rheological behavior of the emulsion gel was studied. This study thus reports a novel application of drug-loaded O/W emulsions for 3D printing of solid oral dosage forms.

2. Materials and methods

2.1. Materials

Maisine CC (mixed long-chain glycerides) was kindly provided by Azelis (Herlev, Denmark). Methocel A4M (methylcellulose), Methocel E4M (hydroxypropyl methylcellulose), and Ac-Di-Sol SD-711 (croscarmellose sodium) were donated by IFF Nutrition & Bioscience. Fasted state simulated intestinal fluid (FaSSIF) powder was purchased from biorelevant.com (Croydon, UK). Analytical solvents were purchased from VWR International (Spånga, Sweden). Soybean oil (long-chain triglycerides), Tween 85, fenofibrate (≥99%), Ludox TM-50 colloidal SiO_2 (22 nm primary particle size specified by manufacturer, 50% w/w suspension in water, negatively charged particles stabilized with sodium counter ions), Nile red, stearic acid (95%), and porcine pancreatin extract (8 × USP specifications activity) were obtained from Merck (Darmstadt, Germany).

2.2. Preparation of formulation

2.2.1. Lipid-based formulation and drug loading

A LBF type I, represented in the lipid formulation classification system, comprising of Maisine CC and soybean oil was prepared as described previously [10,35,36]. The composition is shown in Table 1. Briefly, the components were preheated at 37 °C for soybean oil and at 70 °C for Maisine CC for ~ 30 min until homogenous mixtures were obtained and subsequently weighed into a glass vial in predefined fractions. The vial was vortexed thoroughly and placed on a shaker at

37 °C overnight. A drug loading of 42.2 mg/g (equal to 80% of fenofibrate equilibrium solubility at 25 °C) was prepared by adding the required amount of fenofibrate into a glass vial followed by LBF. The vial was vortexed and placed on a shaker at 37 °C until a clear oil phase was obtained and all drug was dissolved.

2.2.2. Emulsion

An O/W emulsion was prepared using drug loaded LBF as oil phase (Fig. 1a–b, Table 1). Stearic acid (2% w/w) was added as a co-emulsifier to the oil phase by weighing stearic acid directly into a glass vial followed by addition of drug loaded LBF. The vial was vortexed and placed on a shaker at 37 °C overnight. Before use, the oil phase was placed at 70 °C for 15 min to ensure complete dissolution of stearic acid. The aqueous continuous phase, comprising a SiO_2 suspension (15% w/w) in water, was prepared by dilution of Ludox TM-50 colloidal SiO_2 with Milli-Q water, followed by pH adjustment to 7.0 using 0.1 M HCl. The SiO_2 suspension was stored at 4 °C prior to use. The oil and water phases were weighed into a falcon tube in a 3:7 ratio and emulsified using a two-step process to achieve submicron droplet sizes. First, the O/W mixture was ultrasonicated using a Vibra-Cell sonicator equipped with a 13 mm probe tip (Sonics, Newton, CT, USA). An amplitude of 20%, pulse of 30 s on and 1 s off was applied for 5 min. In the second step, the pre-emulsion was processed in a microfluidizer (LM20, Microfluidics, Westwood, MA, USA) with a diamond interaction chamber assembly (H10Z, 100 μm). The pre-emulsion was processed 10 times at 2000 bar. The produced emulsion was stored at room temperature before use.

2.2.3. Emulsion gel

An emulsion gel was prepared from the emulsion (Fig. 1c) by adding viscosity enhancers, Methocel A4M and E4M, and disintegrant, Ac-Di-Sol SD-711. The final composition of the gel is shown in Table 1. The required amount of emulsion was weighed into a glass vial and pre-heated to 70 °C, followed by gradual addition of polymer between cycles of vortexing and re-heating the emulsion. Methocel A4M was added first, followed by Methocel E4M, and lastly, Ac-Di-Sol SD-711. The final gel was stored at room temperature until 3D printing. A previously described emulsion gel using an emulsified LBF type II stabilized with a non-ionic surfactant was used in this study for comparison of textural properties and rheological characteristics important for 3D printing [34]. The composition is shown in Table 1. The LBF type II emulsion gel was prepared according to a previously described method [34].

2.3. Emulsion stability and droplet size measurement

Kinetic stability of the emulsion was assessed over four weeks of storage at room temperature. The emulsion was visually evaluated for potential phase separation by staining the oil phase with Nile red. The volume size distribution and hydrodynamic diameter of the emulsion was measured using dynamic light scattering (DLS; Litesizer 500, Anton Paar GmbH, Graz, Austria). Emulsion samples were diluted 100-fold in Milli-Q water prior to measurement. Droplet size was determined at

25 °C, using a refractive index of 1.5 and absorbance coefficient of 0.005. Droplet size was measured directly after preparation and after four weeks of storage at room temperature. The same parameters (temperature refractive index, and absorbance coefficient) used for DLS measurements of the emulsion was used to measure the particle size of the SiO_2 suspension (15% w/w). Additionally, the zeta potential of the aqueous phase (15% w/w SiO_2 suspension in water) was measured at 25 °C and pH 7.0 (Litesizer 500, Anton Paar GmbH, Graz, Austria).

2.4. Cryo-scanning electron microscopy (cryo-SEM)

Cryo-scanning electron microscopy (cryo-SEM) was used to study the adsorption of SiO_2 nanoparticles at the oil/water interface. Imaging was performed on a low-voltage field-emission cryo-SEM (Carl Zeiss Merlin, Oberkochen, Germany) with a Quorum Technologies PP3000T cryo-preparation system. Emulsion samples were vortexed and frozen in the 100 μm side of a type A 6 mm carrier using a Leica HPM100 high pressure freezing system (Leica microsystems, Wetzlar, Germany). Prior to imaging, samples were stored in liquid nitrogen. Imaging was carried out at −140 °C using a secondary electron detector (ETD) at an accelerating voltage of 1 kV and probe current of 50 pA.

2.5. In vitro lipolysis and drug distribution

In vitro lipolysis of the emulsion and the corresponding LBF type I (50% w/w soybean oil and 50% w/w Maisine CC) was performed according to a previously described protocol [36]. The set-up used consisted of a temperature-controlled glass vessel (37 °C) and a pH-stat (iUnitrode) connected to a dosing unit (Metrohm 907 Titrando, Switzerland). The medium consisted of lipolysis buffer (pH 6.5, containing 2 mM Tris–maleate, 1.4 mM $CaCl_2 \cdot 2H_2O$, and 150 mM NaCl) supplemented with FaSSIF powder (3.0 mM sodium taurocholate and 0.75 mM lecithin). The lipolysis medium was preheated to 37 °C prior to experiments. A pancreatic enzyme extract was prepared by mixing 1.2 g porcine pancreatin, 6 mL lipolysis buffer, and 20 μL 5 M NaOH. The mixture was vortexed and then centrifuged at 5 °C, 2442 *g* for 15 min. The enzyme extract was prepared 1–2 h before use and kept cold until use. The enzyme activity was determined to 36.8 TBU/mg, equal to 7360 TBU/mL extract. At the start of the experiment, a dispersion phase was carried out, where the formulation and lipolysis medium were mixed for 10 min at 450 rpm. The amount of oil and initial volume were the same for experiments carried out with LBF type I and emulsion. For LBF type I, 1.18 g was dispersed in 42.5 mL lipolysis medium and for emulsion, 4.0 g was dispersed in 39.7 mL medium. During the dispersion phase, the pH was manually adjusted to 6.5 ± 0.05. At the end of the dispersion phase, 10 μL was withdrawn to determine the droplet size prior to digestion using DLS. Prior to measurement, the sample was diluted 100-fold in Milli-Q water and measured at 25 °C. The result was analyzed based on the intensity distribution.

To start the digestion phase, 4.5 mL pancreatic enzyme extract was added. The digestion was carried out for 60 min and the pH was

Table 1
Formulation composition of lipid-based formulations (LBFs) type I and II used as oil phase, oil-in-water (O/W) emulsions with particle or surfactant stabilization, and emulsion gels.

LBF			O/W emulsion					Emulsion gel	
Type	Composition (% w/w)		Drug loading[a] (mg/g)	Type of stabilization	O/W ratio	Stearic acid (% w/w)	Silica suspension (% w/w)	Excipient (% w/w)	
I	Soybean oil	50	42.2	Solid particles and surfactant	3:7	2	15	Methocel A4M	6
	Maisine CC	50						Methocel E4M	2
								Ac-Di-Sol SD-711	5
II[b]	Soybean oil	32.5	45.0	Surfactant	3:7	n/a	n/a	Methocel A4M	12
	Maisine CC	32.5						Ac-Di-Sol SD-711	5
	Tween 85	35.0							

[a]Drug load corresponds to 80% of the equilibrium solubility of fenofibrate at room temperature.
[b]A previously described LBF type II emulsion gel was used as a reference gel in this study [34].
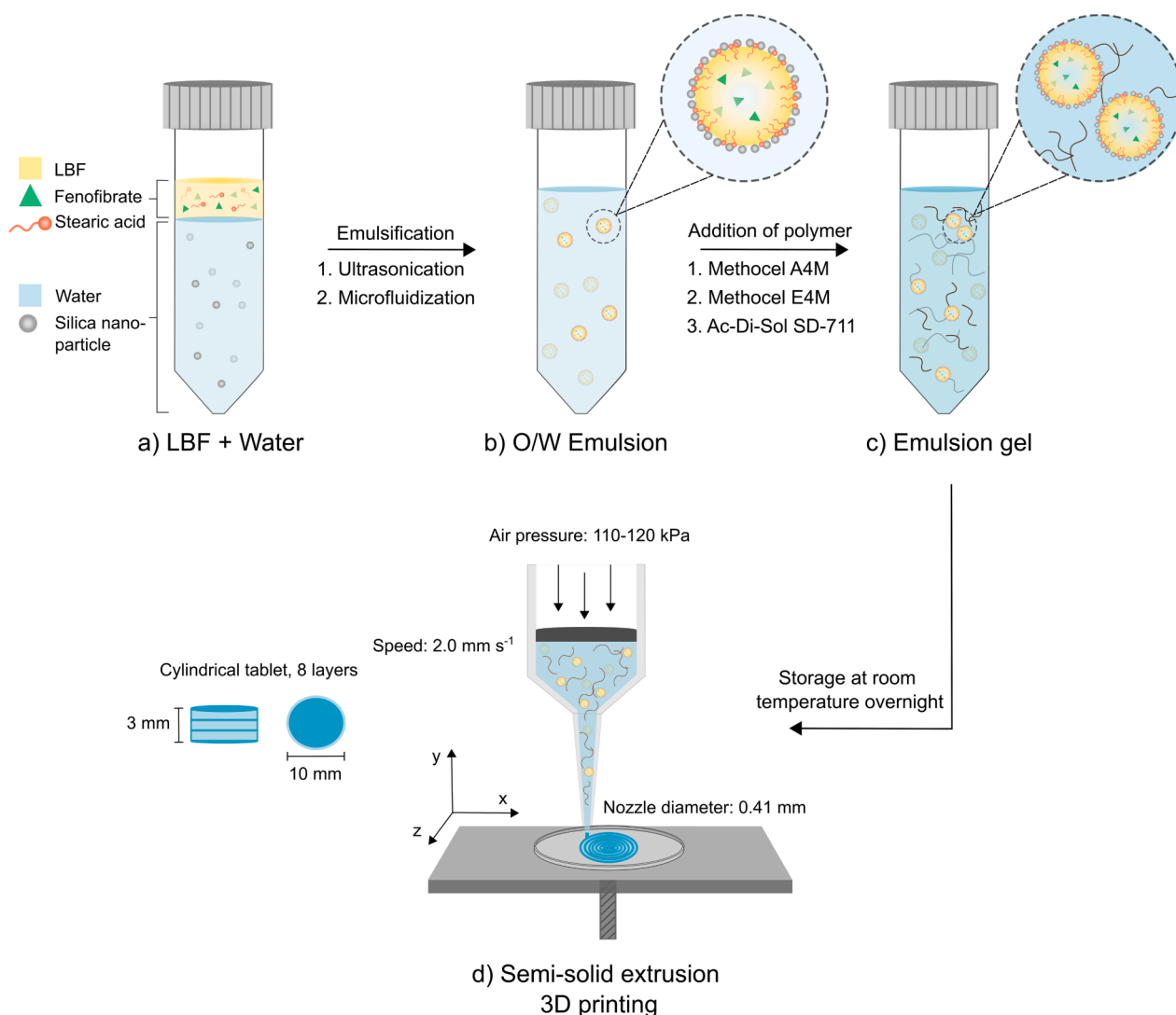
Fig. 1. Experimental schematic of the preparation procedure of emulsion gel stabilized by solid particles and surfactant followed by semi-solid extrusion (SSE) 3D printing into tablets. (a) Drug-loaded lipid-based formulation (LBF) type I (oil dispersed phase) supplemented with stearic acid was added to a silica water suspension (aqueous continuous phase). (b) An oil-in-water (O/W) emulsion was prepared using a two-step procedure. (c) Polymers, two functioning as viscosity enhancers and one as disintegrant were added to transform the emulsion into a printable gel. (d) The emulsion gel was stored at room temperature prior to SSE 3D printing into tablets.

maintained at 6.5 by automatic titration of 0.2 M NaOH from the dosing unit. During the lipolysis experiment, samples of 1 mL were withdrawn after 5 and 10 min of dispersion and 5, 10, 30, and 60 min of digestion. Withdrawn samples were transferred to Eppendorf tubes with 5 μL of lipase inhibitor (0.5 M 4-bromophenyl boronic acid in methanol), vortexed, and centrifuged at 37 °C, 21 000 g for 15 min to separate the three resulting phases; oil, aqueous, and pellet phase. The oil droplets (top layer) were withdrawn with a syringe, transferred to a 5 mL volumetric flask, and dissolved in 2-propanol. The aqueous phase was transferred to a new Eppendorf tube, leaving the pellet in the original tube. The pellet was dissolved in 1 mL of acetonitrile, vortexed, and centrifuged at 22 °C, 21 000 g for 15 min before the supernatant was further diluted. All three phases were diluted 5–20 fold in acetonitrile before drug quantification using HPLC-UV (section 2.10.). After lipolysis, the extent of lipid hydrolysis was estimated by simplifying a previously described equation by Williams and colleagues [36]:

$$\text{Extent digestion (\%)} = \frac{\text{Ionized FAs}}{\text{Theoretical FAs in formulation}} \times 100 \qquad (1)$$

where the quantity of ionized fatty acids (FAs; pH 6.5) determined

from the titrated amount of NaOH during *in vitro* lipolysis is related to the theoretical maximum quantity of FAs that can be released from the formulation during digestion. The estimation assumed that one triglyceride molecule releases two FAs, while diglycerides and monoglycerides release one FA each. According to the certificate of analysis for Maisine CC, the glyceride content was 33% monoglycerides, 50.5% diglycerides, and 15.8% triglycerides. For soybean oil the estimation was based on 100% triglyceride content.

2.6. Rheological characterization

Rheological properties of the emulsion gel were characterized at 20 °C using a Discovery HR-3 rheometer (TA Instruments, New Castle, DE, USA) equipped with a 20 mm stainless steel parallel plate geometry. A solvent trap was used to limit evaporation during experiments. Viscosity was measured under continuous flow, ramping the shear rate from 0.1 to 200 s^{-1} over 10 min after an initial 60 s conditioning time at 20 °C. Flow sweep data for the LBF type I emulsion gel was recorded at a gap of 500 μm while the LBF type II emulsion gel was measured at 250 μm. Amplitude and frequency sweeps were performed at a gap of 500

μm. Amplitude sweeps were performed at 1 Hz by increasing the oscillation strain from 0.01 to 100% strain to determine the linear viscoelastic region. The apparent yield stress was calculated by plotting the storage modulus versus shear stress curves from the amplitude sweeps as described by De Graef and colleagues [37]. Frequency sweeps were performed from 0.01 to 63 Hz at 0.1% strain (within the linear viscoelastic region). The frequency dependence of the gels was evaluated by fitting the data to a power law model:

$$\log(G') = K' + z*\log(\omega) \tag{2}$$

where G' is the storage modulus, ω the angular frequency and the values of z and K' reflect the frequency dependence and structural strength of the sample [38,39].

2.7. Semi-solid extrusion 3D printing

SSE 3D printing was carried out using a BIO X 3D printer (CELLINK, Gothenburg, Sweden) equipped with a pneumatic printhead (Fig. 1d). The emulsion gel was filled into a 3 mL cartridge mounted with a nozzle tip (Ø 0.41 mm). The 3D design used for printing was a cylindrical model with a diameter of 10 mm, height of 3 mm, 8 layers, and 100% infill density. SSE was performed at room temperature and the tablets were printed directly on a glass petri dish using a printing pressure of 110–120 kPa and a printing speed of 2 mm/sec. After SSE 3D printing, the tablets were dried in a vacuum oven at 22 °C, 400 mbar overnight (Vacutherm, Thermo Fisher Scientific, Massachusetts, USA). Following vacuum drying, the tablets were air dried for another 24 h. The mass of each tablet was recorded after drying. The diameter and thickness of dried tablets were measured using a digital micrometer (QuantuMike IP65, Mitutoyo, Japan).

2.8. Texture profile analysis

Texture profile analysis of 3D-printed tablets was carried out using a TA.XT plusC texture analyzer (Stable Micro Systems Ltd, Godalming, United Kingdom). The analysis was conducted in a double compression test mode at room temperature. A compression plate, 35 mm in diameter was used to compress the soft dosage forms to 30% strain deformation. The pre-test and post-test speeds were set to 1.5 mm/sec, while the compression rate was 1.0 mm/sec. The delay time between the first and second compression cycle was 5 s with a 5 g trigger force. Force versus time plots were generated and textural parameters (hardness, adhesiveness, cohesiveness, springiness, and gumminess) were determined using Exponent Connect software (version 8.0.7.0, Stable Micro Systems Ltd, Godalming, United Kingdom).

2.9. Tablet disintegration time

The disintegration time of 3D-printed tablets was assessed using a disintegration instrument (PTZ AUTO 1EZ, Pharma Test, Hainburg, Germany) equipped with a PT-MKT electronic disintegration basket and temperature sensor. In total, six tablets were placed, one in each of the glass cylinders, followed by adding a disk on top of the tablet. The basket assembly was then immersed in a beaker filled with ~ 800 mL of water. The disintegration test was performed at 37.0 ± 0.5 °C, 30 cycles/min, for 15 min or until all tablets had disintegrated. The disintegration time of each individual tablet was automatically recorded.

2.10. Drug content analysis

The drug recovery in the emulsion was analyzed for potential drug loss during the formulation process. In short, ~ 100 mg of emulsion was weighed into 5 mL volumetric flasks and diluted with 2-propanol. The samples were further diluted 10-fold in acetonitrile, followed by 5-fold dilution in mobile phase prior to drug quantification. Drug content in

3D-printed tablets were analyzed by dispersing the tablets in 40–50 mL of Milli-Q water under stirring for 45 min. Samples of 1 mL were withdrawn, transferred to 5 mL volumetric flasks and subsequently diluted in 2-propanol. The samples were diluted 2-fold in mobile phase.

Prior to drug quantification, samples containing emulsion were filtered using 0.02 μm syringe filters to remove potential SiO$_2$ particles. All samples were centrifuged, 22 °C, 21 000 g for 15 min, and ~ 500 μL of the supernatant was transferred to HPLC vials. Analysis was carried out using an HPLC (1290 Infinity, Agilent Technologies, Santa Clara, CA, USA) with a Zorbax Eclipse XDB-C18 column (4.6 × 100 mm). The analytical conditions used was an isocratic flow rate of 1 mL/min, injection volume of 20 μL, and the column temperature was set to 40 °C. The mobile phase consisted of acetonitrile:sodium acetate buffer (25 mM, pH 5.0) at the ratio 80:20 (v/v). UV absorbance for fenofibrate was measured at a wavelength of 287 nm and the retention time was 3.12 min. Calibration curve and quality control samples (used to assure accuracy of analysis) were used in a range between 0.78 and 100 μg/mL.

3. Results and discussion

3.1. Emulsion

3.1.1. Emulsion stability and morphology

The properties of the solid particle stabilizer, including wettability, size, shape, and concentration are crucial to the stability of Pickering emulsions [13,40–42]. In our study, an emulsion synergistically stabilized with stearic acid and SiO$_2$ nanoparticles was formulated (Table 1). The hydrodynamic diameter of the SiO$_2$ nanoparticles was measured to 29.4 ± 1.7 nm (Fig. S1), which is slightly larger than the 22 nm specified by the manufacturer. The zeta-potential of the particles at pH 7.0 was measured to – 31.6 ± 3.2 mV. The physical stability of the emulsion was assessed by measuring the volume size distribution over four weeks of storage (Fig. 2a). The hydrodynamic diameter of freshly prepared emulsion and after storage was 341 nm and 361 nm, respectively, and the polydispersity index (PDI) was < 0.2 for both time points (Table S1), demonstrating emulsion stability for at least one month at room temperature. In addition, no phase separation was observed visually for the emulsion with stained oil phase (Fig. S2).

The size of the stabilizing particle influences the emulsion droplet size, where a smaller size favors the formation of smaller emulsion droplets [40]. In addition to particle size, the particle charge, concentration, and emulsification process affect the final droplet size [15,43]. The SiO$_2$ particles and steric acid were negatively charged at pH 7.0, used in the aqueous phase. Negatively charged SiO$_2$ nanoparticles and surfactants have previously been used to stabilize water-in-oil emulsions [44]. Furthermore, both ultrasonication and microfluidization that were used during emulsification are energy intensive processes contributing to the small droplet size obtained. A small droplet size is desirable due to its strong correlation with high stability. Surfactant-stabilized emulsions typically exhibit smaller droplet sizes. For example, in a previous study, a lipid mixture of soybean oil and Maisine CC (LBF type II) had a hydrodynamic diameter of 103 nm after emulsification with the nonionic surfactant tween 85 [34]. However, due to the high energy required to remove particles from the oil–water interface, Pickering emulsions with significantly larger droplet sizes than reported here have shown long-term stability against droplet coalescence [15]. The hydrophilic colloidal nanoparticles used here were not modified further. Modification of colloidal particles using e.g., chitosan or charged low-molecular weight amphiphilic molecules have previously been applied to adjust the hydrophobicity and thereby tune particle wetting behavior for optimal interfacial adsorption [15,45]. In addition to particle stabilization, the emulsion developed here was co-stabilized by stearic acid. A synergistic stabilization of emulsions using a combination of nanoparticles and surfactants has previously been demonstrated [44,46]. It should be noted that control emulsions prepared with only SiO$_2$ nanoparticles or stearic acid were not stable and phase separation was
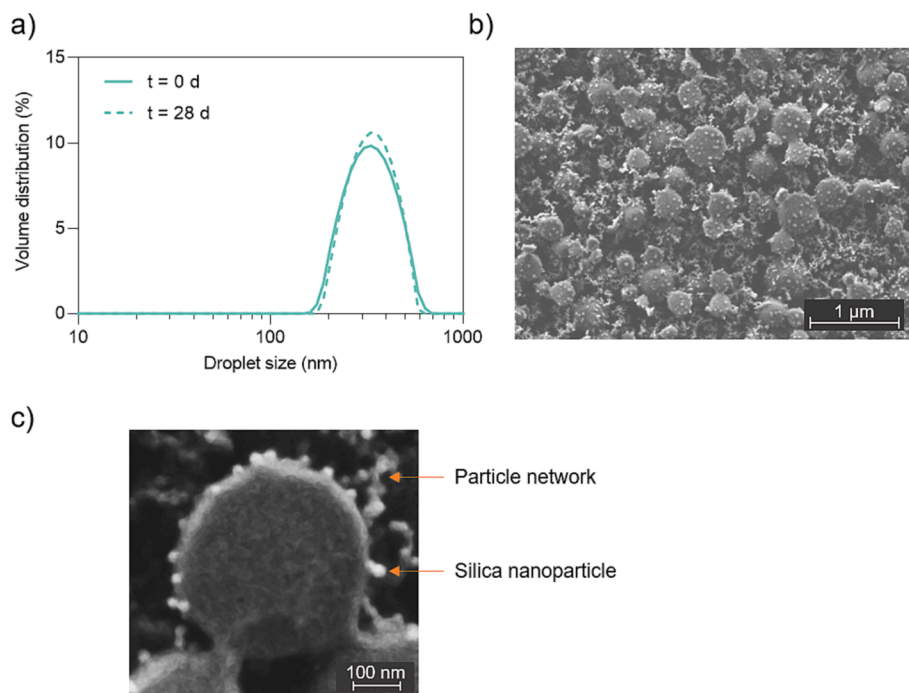
Fig. 2. Characterization of oil-in-water emulsion. (a) Droplet size distribution of emulsion after preparation (solid line) and after 28 days of storage at room temperature (dashed line). Values are expressed as mean (n = 3). (b–c) Cryo-SEM images of emulsion showing silica nanoparticles adsorbed to the oil–water interface and particle network between oil droplets.

observed within 24 h. This emphasizes the synergistic stabilization of nanoparticles and the surfactant in the developed emulsion here (Fig. 2a).

The emulsion morphology was visualized by cryo-SEM (Fig. 2b–c). A partial coverage of the oil droplet surface with SiO_2 nanoparticles was observed. The theoretical surface coverage of SiO_2 based on hexagonal close packing of hard circles was estimated to 47.2% [47] (section 3, supplementary material), which confirms a partial surface coverage of the particles. Experimentally determined surface coverage is typically lower than this theoretical value. Residual silica in the aqueous phase of the emulsion is often obtained [47], as qualitatively observed here also in SEM (Fig. 2c). Furthermore, electrostatic repulsions between adsorbed particles at the interface prevent their close packing, especially at pH 7 used here for emulsification. Finally, particles often adsorb in clusters or aggregates rather than primary particles to the interface. These factors contribute to a lower surface coverage than the maximum predicted by theory. Adsorbed particles function as a steric barrier against droplet coalescence. A low surface coverage can favor bridging or networking of droplets by simultaneous adsorption of one particle to two emulsion droplets [15,48]. The emulsion is stabilized by both particle and network mechanisms and thus contributes to the stability observed [15]. The coverage at the oil–water interface is influenced by the particle concentration. Previous studies have reported a reduction in size of the emulsion droplets with increased concentration of particles, resulting in improved stability [49,50]. The concentration of SiO_2, 15% (w/w) in the aqueous phase in our study was optimized from lower levels (7% w/w; droplet size of 521 nm) to reduce droplet size and improve stability. A partial coverage at the oil–water interface was desirable to facilitate the interfacial process of lipid digestion (section 3.1.2.). In summary, an emulsion stable for at least one month was produced with SiO_2 particles adsorbed at the oil–water interface to stabilize the emulsion. Furthermore, the developed formulation allows for an LBF type I to be transformed into an emulsion with submicron droplets, incorporating a poorly water-soluble drug, to enable rapid digestion and drug release.

3.1.2. In vitro lipolysis

A standard pH-stat lipolysis model was used to evaluate the digestion, central for *in vivo* performance of lipid-based drug delivery systems. Fig. 3a shows the extent of lipid digestion during 60 min of lipolysis of the emulsion and the corresponding LBF type I without emulsion stabilization dispersed as it is in the lipolysis medium. The initial rate of digestion for emulsion was rapid, showing a steep increase during the first 10 min of digestion. A plateau in extent of digestion of 15% was reached after ~ 15 min. The corresponding LBF type I showed a slower digestion rate compared to the emulsion, reaching a total extent of digestion of 13% after 60 min of digestion. The extent of digestion for the LBF type I included here was lower than previously reported, where an extent of 25% was demonstrated following 30 min digestion of an LBF type I comprising long-chain lipids [36]. The lower extent shown in our study is most likely due to the incomplete ionization of FAs at pH 6.5. For long-chain LBFs, the majority of liberated FAs during digestion have been shown to be unionized at pH 6.5 by adding a back-titration step, increasing the pH to 9.0 at the end of the experiment. For a long-chain LBF type I, a unionized-ionized FA ratio of 5.0 was reported [36]. Taking the unionized FAs into account, the extent of digestion for both emulsion and LBF can be assumed to be higher than reported here.

A central aspect influencing the lipid digestion kinetics is the droplet size [51,52]. Following dispersion, the LBF type I formed a coarse emulsion with a droplet size of several micrometers (PDI of 0.4). For comparison, the emulsion had a droplet size of < 500 nm (PDI of 0.2) prior to the digestion phase (Fig. S3a-b, Table S2). The smaller droplet size of the emulsion resulting in a larger surface area for binding of lipase to the oil–water interface can explain the more rapid lipid digestion observed for this formulation (Fig. 3a) [53]. The presence of interfacial colloidal particles in the emulsion is another important aspect to consider when comparing the digestion profiles. Lipolysis is an interfacial process governed by the competitive binding of lipase/colipase and bile salts at the oil–water interface. In the case of Pickering emulsions, the particles form an energy barrier, which hinder lipase binding and activity. In a previous study, it was reported that SiO_2 particles reduced the overall extent of digestion, but did not affect the
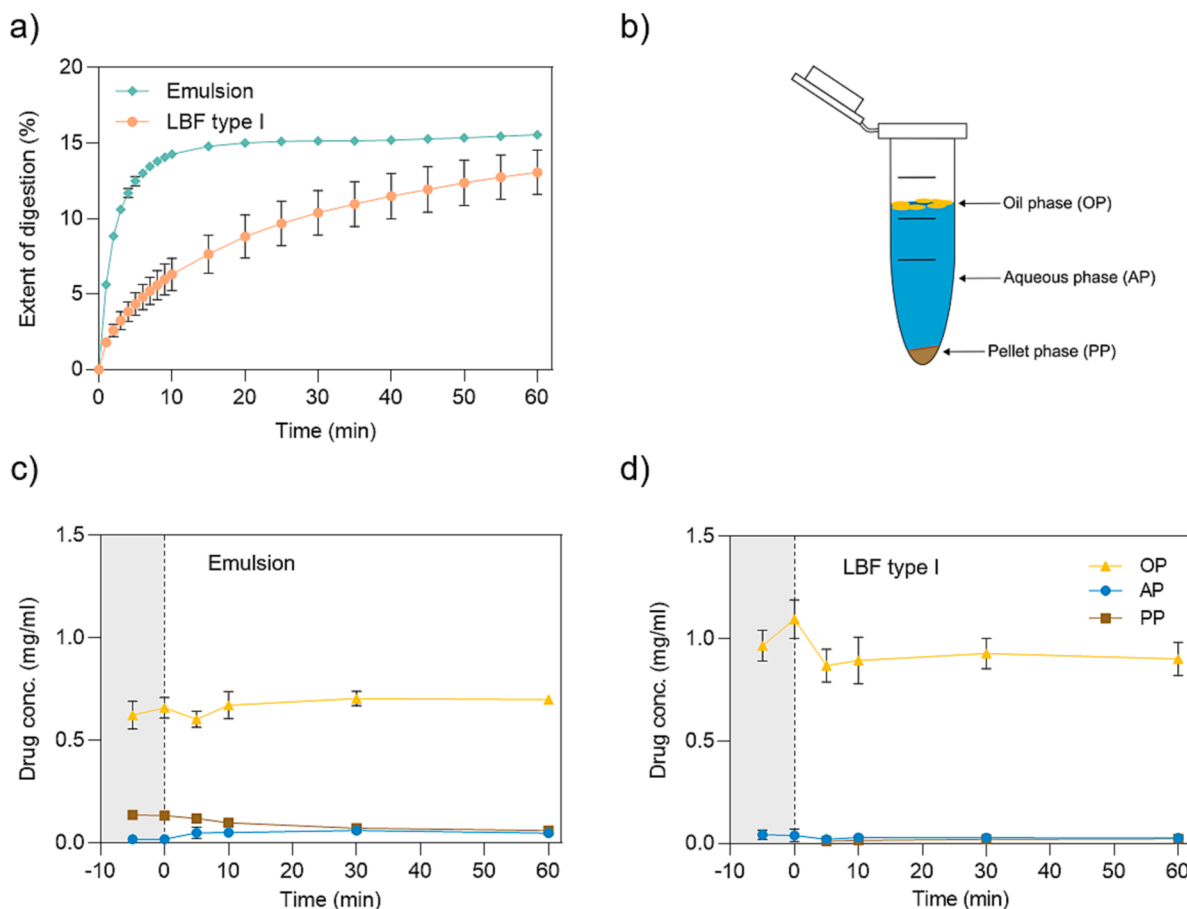
Fig. 3. Digestion profiles and drug distribution during *in vitro* lipolysis of emulsion and corresponding lipid-based formulation (LBF) type I. (a) The extent of digestion during 60 min of *in vitro* lipolysis of LBF type I emulsion (stabilized with SiO_2 nanoparticles and stearic acid) and pure lipid-phase LBF type I without emulsion stabilization. (b) Schematic of an Eppendorf tube after centrifugation illustrating the three separated phases; oil phase (OP), aqueous phase (AP), and pellet phase (PP) analyzed for drug concentration during *in vitro* lipolysis. The drug can be present as solubilized in either the OP or AP, or as precipitated drug in the PP. (c–d) Distribution of drug during dispersion phase (grey shaded area) and digestion phase (white area) of (c) emulsion and (d) LBF type I. No pellet phase was present during dispersion phase of the LBF type I. Values are presented as mean ± SD, n = 3.

initial rate of digestion compared to an emulsion stabilized with β-lactoglobulin [54]. Furthermore, altering the concentration of SiO_2, 1–5% (w/w) did not influence the rate or extent of digestion in that study. Similarly, curcumin was retained in SiO_2-stabilized Pickering emulsions during simulated gastric digestion and were instead released during intestinal digestion [55]. The digestion of particle-stabilized emulsions has also been compared to that of surfactant-stabilized emulsions. In a previous study, emulsions of medium-chain tri-glycerides and long-chain triglycerides (soy bean and canola oil) Pickering emulsions stabilized by milled cellulose or surfactant-stabilized (conventional emulsions) were evaluated [56]. The result showed a faster initial digestion rate for conventional emulsions compared to Pickering emulsions. However, the total extent of digestion for Pickering emulsions was higher compared to conventional emulsions. The findings suggested that the larger surface area of conventional emulsion promotes rapid initial digestion, but the total extent of digestion might be reduced due to the inhibiting effect of non-ionic surfactants. The inhibitory effect of non-ionic surfactants on the digestion at the lipid interface has also previously been demonstrated [53]. We speculate that the small droplet size and the partial surface coverage of SiO_2 particles at the interface of the emulsion here (Fig. 2b, section 3.1.1.) allowed for sufficient access for lipase and bile salts to the interface for a rapid initial lipolysis as observed. A more rapid digestion compared to the corresponding LBF without any emulsification stabilizer is desirable for a faster drug release.

Bioaccessibility from *in vitro* lipolysis can be assessed by removing

samples during the experiment and analyzing the drug distribution in different phases. Following centrifugation, three phases can be observed; a poorly dispersed oil phase, a colloidal aqueous phase, and a precipitated pellet phase (Fig. 3b). The distribution of the drug in these phases during the dispersion and digestion stages of lipolysis for the emulsion and LBF type I is shown in Fig. 3c–d, respectively. For both formulations, the majority of the drug resided in the poorly dispersed oil phase throughout the lipolysis experiment. The concentration of drug in the oil phase was lower for the emulsion compared to the LBF type I, most likely due to the lower total mass balance across the three phases (Fig. S4a–b). For the LBF type I, the drug concentration in the aqueous phase and the amount of precipitated drug were low (Fig. 3d). This is consistent with previous studies [36,57,58] and reflects the incomplete digestion and poor emulsification efficiency of this highly lipophilic LBF, where the high affinity of fenofibrate to the lipid components limits drug transfer to the aqueous phase. This further demonstrates the ability of lipid-rich LBFs to keep the drug solubilized during digestion with low risk of drug precipitation. This is due to a low supersaturation level in the aqueous phase compared to the more hydrophilic LBFs (type II–IV), which are more rapidly digested [36,57].

The concentration of drug in the aqueous phase for Pickering emulsion was slightly higher than that of the LBF and increased during lipolysis. This might be due to the more rapid and higher extent of digestion leading to a higher amount of drug being released and solubilized in the aqueous phase. However, a higher amount of drug was also observed to have precipitated in the pellet phase for the emulsion, where

a pellet phase was observed both during dispersion and digestion (Fig. 3c, S5a–b). In contrast, no pellet phase was observed during dispersion of the LBF type I (Fig. 3d, S4b). Precipitation of drug during dispersion of the emulsion was unexpected due to the solubilization capability of this type of LBF and the relatively modest drug loading used (80% of the equilibrium solubility). No precipitation of drug after emulsification was observed and the drug recovery of prepared the emulsion was ≤ 5% deviation from the theoretical concentration (Fig. S6), indicating that no drug precipitate was present after emulsification. The amount of precipitated drug during lipolysis of the emulsion decreased during lipolysis (Fig. 3c, S4a), indicating that the precipitated drug dissolved during lipolysis and was not further triggered by digestion. The *in vivo* relevance of drug precipitation *in vitro* can be discussed*,* where previous studies have demonstrated an overestimation of drug precipitation from *in vitro* lipolysis studies [59–61], reflecting the absence of an absorptive compartment in this standard setup. In summary, the emulsion was more rapidly digested compared to the corresponding LBF type I, with most of the drug recovered solubilized in the oil phase during digestion.

3.2. Emulsion gel

3.2.1. Printable formulation

The emulsion was transformed into an emulsion gel by addition of cellulose biopolymers. A combination of 6% (w/w) Methocel A4M (methylcellulose) and 2% (w/w) Methocel E4M (hydroxypropyl methylcellulose) (Table 1), was used to produce a formulation with suitable rheological attributes for SSE 3D printing into tablets. Individual use of these cellulose polymers has previously been studied for production of tablets using SSE [21,34,62]. A combination of methylcellulose and hydroxypropyl methylcellulose was selected based on a pre-screening of different cellulose polymers and combinations of these (Table S3). Several polymer compositions were printable, however often oil leakage from the tablets after printing was observed. The composition used for further study was selected based on printability and the absence of oil leakage after printing. Ac-Di-Sol SD-711 (croscarmellose sodium) was added as a disintegrant at 5% (w/w), to achieve rapid tablet

disintegration as previously demonstrated for 3D-printed tablets from emulsion gels [34].

3.2.2. Rheological properties

The extrudability and printability performance of a semi-solid material by SSE 3D printing is governed by its rheological properties, such as viscosity, shear-thinning response, elastic properties, and yield stress [20]. The flow behavior and apparent viscosity of the emulsion gel is shown in Fig. 4a. For comparison, an LBF type II emulsion gel (stabilized only by surfactants) from a previous study [34] was included and the corresponding result is shown in Figure S7a. Shear rates above 63 s⁻¹ were excluded due to problems with sample flowing out of the geometry at higher shear rates. A lower gap was used for the LBF type II emulsion gel due to the increased range of shear rates that could be measured without sample escaping the geometry. Both the LBF type I and the LBF type II emulsion gels showed a shear-thinning behavior with decreasing viscosity as the shear rate was increased. The shear-thinning behavior can be explained by the reorganization of the macromolecular polymer network reducing the viscosity during shearing. This is favorable in extrusion-based 3D printing, as it allows for flow of the material through a small nozzle upon application of an external force [21,63]. In addition to shear-thinning behavior, the viscosity of an ideal soft material should be rapidly recovered after removing the stress or shear rate to ensure high shape fidelity and to avoid deformation of the structure after deposition [64]. The LBF type I emulsion gel showed a higher viscosity throughout the range of shear rates measured, compared to the LBF type II emulsion gel. A higher apparent viscosity with increasing concentration of cellulose biopolymers has previously been demonstrated [21,62,63]. The emulsion gels included here contained in total 8% (w/w) and 12% (w/w) cellulose for LBF type I and type II emulsion gels, respectively (Table 1). The lower total amount of polymer for the LBF type I emulsion indicates that the higher viscosity observed for this emulsion gel is related to other compositional differences, e.g. the presence of nanoparticles in the formulation. An increasing content of SiO₂ particles in emulsions has previously been correlated to increased viscosity [65].

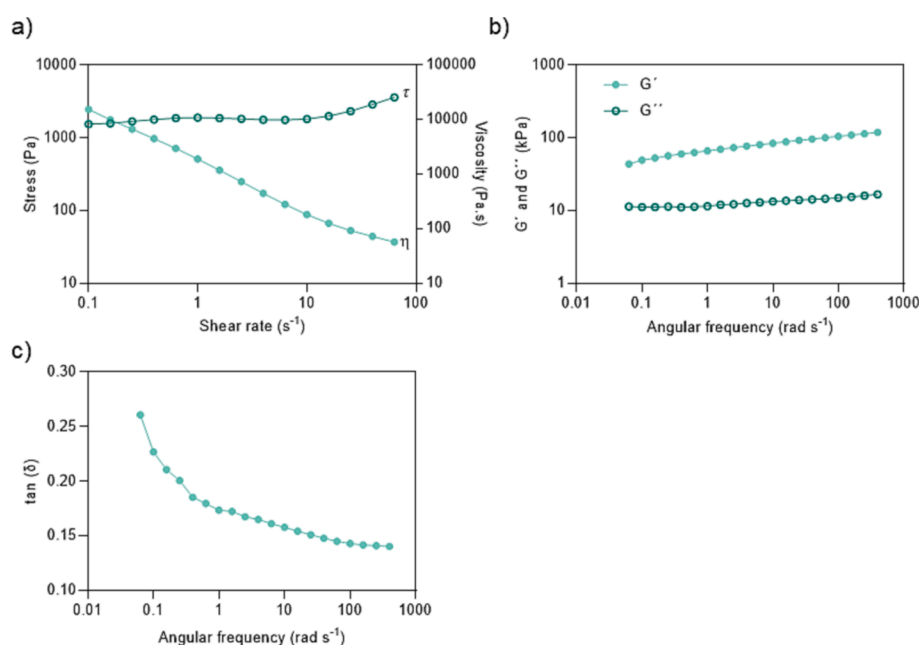Different fluid models (Herschel-Bulkley fluid, Newtonian, Bingham,

Fig. 4. Rheological properties of LBF type I emulsion gel. (a) Shear stress (τ, open symbols) and apparent viscosity (η, closed symbols) as a function of shear rate. (b) Storage modulus (G′, closed symbols) and loss modulus (G″, open symbols) versus angular frequency profiles. (c) tan δ (G″/G′) as a function of the angular frequency. Values are presented as mean of two measurements.

Casson, and Power law) were fitted to the flow sweep data of the LBF type I emulsion gel. However, none of the investigated models were able to accurately capture the behavior of this gel, hence giving a poor fit to the models ($R^2 < 0.94$). This was mainly due to the small peak in shear stress at a shear rate around one that was observed for this gel (Fig. 4a). For the LBF type II emulsion gel the data fit the Herschel-Bulkley fluid model well ($R^2 > 0.99$) with a flow behavior index (n) <1, indicating that the material was shear-thinning (Table S4). Differences observed for the LBF type I emulsion gel could potentially be the result of difficulties with measuring high viscosity samples using rotational rheology due to artefacts caused by e.g., shear fracturing and wall slip [64].

Amplitude sweeps were performed to determine the linear viscoelastic region and yield stress of investigated gels (Table 2). The yield stress can be defined as the threshold stress above which the material starts to break down and flow is induced, and hence can be used as an indication of the minimum pressure needed for extrusion. A higher apparent yield stress was recorded for the LBF type I emulsion gel compared to the LBF type II emulsion gel, which further correlates with a higher printing pressure needed for extrusion; 110–120 kPa compared to 55 kPa (Table 2). For the purpose of 3D printing, a high yield stress can lead to problems due to the need of high printing pressures. On the other hand, a high yield stress has been linked to a better shape retention after printing [62,64]. Yield stress has previously been shown to increase with increasing cellulose polymer concentration [21,62]. The higher yield stress observed for the LBF type I emulsion gel containing a lower polymer concentration further suggest the influence of other components in the composition on its rheological properties. Previously, SiO_2 particles have been shown to influence the yield stress of an emulsion, where increased amount resulted in higher yield stress [65].

Furthermore, the rheological properties of the gels were characterized by a frequency sweep (Fig. 4b–c, S7b–c). The storage modulus (G′) can be described as representing the elastic behavior of a formulation, and the loss modulus (G″) represents the viscous behavior. Both emulsion gels showed a G′ higher than G″ over the full frequency range measured indicating that the gels had an elasticity dominated gel-like structure [21,64]. The LBF type I emulsion gel showed a higher G′, indicating a stronger mechanical strength than the surfactant-stabilized LBF type II emulsion [62]. The parameter tan δ is the ratio between G″ and G′, i.e., the ratio of the viscous and elastic portion of the viscoelastic deformation behavior. As seen from Fig. 4c and S7c, a lower tan δ was recorded towards higher angular frequencies for both emulsion gels, indicating a more solid-like behavior [21]. Frequency data was fitted to the power law equation to characterize the frequency dependence of the gels, with K′- and z-values reported in Table 2. As expected, K′-values follow the same trend as the logarithm of G′. Both emulsion gels, LBF type I and II, showed a similar dependence on frequency, as indicated by the small differences in z-values. Overall, a trend of higher viscosity, yield stress, and G′ was observed for the LBF type I emulsion gel synergistically stabilized by nanoparticles and stearic acid, compared to the surfactant-stabilized LBF type II emulsion gel. These observations might be explained by a strong bridging particle network between droplets formed at higher SiO_2 concentration [15]. Such particle networks have previously been shown to increase the viscosity and yield stress of the material [65]. The formation of an agglomerated network was further shown to be critical to forming an ideal emulsion for 3D printing,

displaying high yield stress, storage modulus, and elastic recovery.

3.3. 3D-printed tablets

3.3.1. 3D printing and physical parameters

The LBF type I emulsion gel was 3D printed into cylindrical tablets using SSE (Fig. 5a). As shown in the photograph, the 3D-printed tablet retained a good shape after layer-by-layer deposition of the formulation. The good visual appearance of the tablets after printing indicate that the high yield stress (1682 Pa) measured for this formulation resulted in an adequate shape retention ability [62,64]. In addition, despite the relatively high apparent yield stress, the formulation showed acceptable extrudability using a pressure of 110–120 kPa. This is consistent with a previous 3D printing study using hydroxypropyl methylcellulose hydrogels, where they demonstrated that a yield stress < 4000 Pa leads to good extrudability [21]. A post-processing step is often necessary in SSE 3D printing for solidification of the printed tablets. Here, were dried the tablets in a vacuum oven followed by drying at room temperature (Fig. 5b). After drying, the tablets showed a rougher surface texture, most likely caused by water evaporation and tablet shrinkage. The average weight of dried tablets was 142.7 ± 6.0 mg (n = 3). The dry tablets had a diameter of 9.0 ± 0.1 mm and a thickness of 2.8 ± 0.0 mm (n = 3), corresponding to ≤ 10% deviation from the original 3D model used (10 mm diameter × 3 mm height).

3.3.2. Mechanical properties

Texture profile analysis is commonly applied in food sciences to investigate textural properties of food. This technique has also been shown to be suitable for analyzing mechanical properties of soft 3D-printed dosage forms not applicable for standardized pharmaceutical hardness test developed for conventional compressed tablets [21,25,66]. The texture profile analysis parameters (hardness, adhesiveness, cohesiveness, springiness, and gumminess) of 3D-printed tablets from LBF type I emulsion gel and LBF type II emulsion gel are shown in Table 3. For comparison, analysis was also carried out on soft candy gummy bears and chewable pastilles (Table S5). Hardness can be described as the force required for a material to deform under
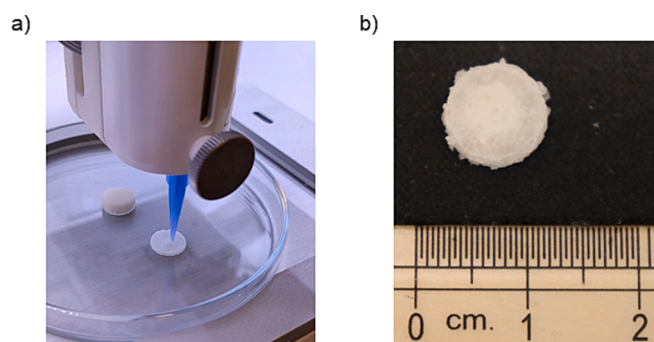
a)   b)

Fig. 5. Images of 3D-printed tablets consisting of LBF type I emulsion gel. (a) Image of semi-solid extrusion 3D printing of emulsion gel into tablets. (b) Image of 3D-printed tablets after drying with scale bar in the bottom.

Table 2

Rheological characteristics and printing parameters for lipid-based formulation (LBF) type I emulsion gel and LBF type II surfactant-stabilized emulsion gel. The rheological properties presented are apparent yield stress, K′- and z-values were obtained by fitting the frequency sweep data to a power law model. Values are presented as mean of two measurements. Printing parameters presented are the printing pressure and speed used for semi-solid extrusion (SSE) 3D printing.

Formulation		Rheological characteristics			Printing parameters	
Type of emulsion gel	Type of stabilization	Apparent yield stress (Pa)	K′-value	z-value	Pressure (kPa)	Speed (mm/sec)
LBF type I emulsion gel	Solid particles and surfactant	1681.6	4.9	0.1	110–120	2
LBF type II emulsion gel[a]	Surfactant	188.0	4.5	0.1	55	2

[a] A previously described LBF type II emulsion gel was used as a reference gel in this study [34].

Table 3

Mechanical properties from texture profile analysis of 3D-printed tablets consisting of lipid-based formulation (LBF) type I emulsion gel and LBF type II emulsion gel. Values are presented as mean $\pm$ SD (n = 3).

Formulation		Mechanical properties				
Type of emulsion gel	Type of stabilization	Hardness (g)	Adhesiveness (g.sec)	Cohesiveness (%)	Springiness (%)	Gumminess
LBF type I emulsion gel	Solid particles and surfactant	2788.1 $\pm$ 379.1	-0.1 ± 0.0	3.7 $\pm$ 0.4	2.5 $\pm$ 0.4	104.8 $\pm$ 26.6
LBF type II emulsion gel[a]	Surfactant	1998.7 $\pm$ 156.5	-0.1 ± 0.0	2.1 $\pm$ 0.1	2.0 $\pm$ 0.1	41.6 $\pm$ 6.0

[a] A previously described LBF type II emulsion gel was used as a reference gel in this study [34].

compression. The 3D-printed tablets from LBF type I emulsion gel were harder (2788.1 g) compared to those from LBF type II emulsion gel (1998.7 g). This finding is in line with the rheological properties observed for these emulsion gels. A higher yield stress and G', as observed here for the LBF type I emulsion gel, have been correlated to increased hardness [21]. The hardness of SSE 3D-printed tablets can be controlled by the concentration of binder or polymer in the formulation [62,67]. The higher hardness of LBF type I emulsion tablets compared to LBF type II emulsion can be attributed to the presence of the SiO_2 nanoparticles in the former. The hardness of LBF type I emulsion 3D-printed tablets was shown to be in between softer candy gummy bears and harder chewable pastilles (Table 3, S5). LBF type I emulsion tablets showed a low adhesiveness, ranging from -0.5 to 0 g.sec. This indicate low stickiness of the material during compression, as it describes the energy required to overcome the attractive forces between the two surfaces. The cohesiveness and springiness, relating to the ability of the material to withstand deformation under mechanical action and elasticity, respectively, was similar for LBF type I and type II emulsion gel. The last parameter investigated was gumminess, which is only applicable for semi-solid materials. The gumminess of LBF type I emulsion tablet was lower than that of LBF type II 3D-printed tablets; 104.8 and 41.6, respectively (Table 3). Similar to the hardness parameter, the gumminess of LBF type I emulsion gel tablets was in between soft candy gummy bears and chewable pastilles. Overall, the LBF type I emulsion 3D-printed tablets showed good mechanical strength and textural properties that could be related to the rheological properties of the formulation.

3.3.3. Disintegration and drug content

Disintegration of a solid dosage form is the first step in the process of dissolution. The disintegration time of LBF type I emulsion 3D-printed tablets with 100% infill density was measured to 7.62 $\pm$ 1.01 min (n = 6). A quick disintegration, within 15 min for 3D-printed tablets from emulsion consisting of 5% (w/w) Ac-Di-Sol SD-711 in the wet formulation, has previously been demonstrated [34]. The drug content in the final dry 3D-printed tablet from LBF type I emulsion gel was 3.36 $\pm$ 0.13 mg (n = 3,), corresponding to 2.36% (w/w) and $\leq$ 3% deviation from the theoretical drug content (Fig. S6), indicating a good drug recovery in the produced 3D-printed tablets. The dosage in the printed form is directly related to the drug loading capacity of the LBF [36]. The developed formulation is aimed towards oral delivery of highly potent, poorly-water soluble drugs. The choice of fenofibrate as a model compound was based on its physicochemical properties with a logP > 5 and poor solubility in aqueous media, which makes it a well-studied model compound in the formulation of lipid-based drug delivery systems. Thus, the developed method is expected to be translational to other more clinically relevant compounds for therapeutic use.

4. Conclusions

An emulsion with fenofibrate-loaded oil droplets synergistically stabilized by SiO_2 nanoparticles and stearic acid was developed from an LBF type I. The emulsion oil droplets were submicron sized, partially covered with SiO_2 nanoparticles at the oil/water interface, and stable at room temperature for at least one month. The small droplet size and partial surface coverage of solid particles at the interface allowed for a more rapid digestion of the emulsion compared to the corresponding plain LBF type I. The emulsion was successfully formulated into a 3D-printable gel by addition of cellulose biopolymers. The rheological behavior of the LBF type I emulsion gel was compared to a purely surfactant-stabilized LBF type II emulsion gel showing a trend of higher viscosity, yield stress, and G' for the LBF type I emulsion gel. The altered rheological behavior of the LBF type I emulsion gel can be attributed to the bridging of SiO_2 particle network between oil droplets. The LBF type I emulsion gel showed rheological properties suitable for 3D printing into tablets with good appearance, mechanical strength, and rapid disintegration. In summary, this study expands the use of lipid-based drug delivery systems for SSE 3D printing of solid oral dosage forms. The Pickering emulsion approach allows for incorporation of a non-emulsifying LBF type I into solid lipid tablets. Such tablets can be used as an alternative to liquid filled capsules to enable rapid oral delivery of lipophilic, poorly water-soluble drugs. Moreover, by 3D printing the tablets can be further tailored based on specific patient needs.

CRediT authorship contribution statement

Jenny Johannesson: Conceptualization, Methodology, Investigation, Writing – original draft, Visualization. **Malhar Manik Pathare:** Conceptualization, Methodology, Investigation, Writing – original draft, Visualization. **Mathias Johansson:** Methodology, Investigation, Writing – original draft, Visualization. **Christel A.S. Bergström:** Conceptualization, Methodology, Writing – review & editing, Supervision, Funding acquisition. **Alexandra Teleki:** Conceptualization, Methodology, Writing – review & editing, Supervision, Funding acquisition.

Declaration of Competing Interest

The authors declare that they have no known competing financial interests or personal relationships that could have appeared to influence the work reported in this paper.

Data availability

Data will be made available on request.

Acknowledgements

Pharmacy, Uppsala University) for help with SEM imaging.

Appendix A. Supplementary material

Supplementary data to this article can be found online at https://doi.org/10.1016/j.jcis.2023.07.055.

References

[1] C.J.H. Porter, N.L. Trevaskis, W.N. Charman, Lipids and lipid-based formulations: optimizing the oral delivery of lipophilic drugs, Nat. Rev. Drug Discov. 6 (3) (2007) 231–248, https://doi.org/10.1038/nrd2197.

[2] H. Mu, R. Holm, A. Müllertz, Lipid-based formulations for oral administration of poorly water-soluble drugs, Int. J. Pharm. 453 (1) (2013) 215–224, https://doi.org/10.1016/j.ijpharm.2013.03.054.

[3] L.C. Alskär, A. Parrow, J. Keemink, P. Johansson, B. Abrahamsson, C.A.S. Bergström, Effect of lipids on absorption of carvedilol in dogs: Is coadministration of lipids as efficient as a lipid-based formulation? J. Control. Release 304 (2019) 90–100, https://doi.org/10.1016/j.jconrel.2019.04.038.

[4] A.J. Humberstone, W.N. Charman, Lipid-based vehicles for the oral delivery of poorly water soluble drugs, Adv. Drug Deliv. Rev. 25 (1) (1997) 103–128, https://doi.org/10.1016/S0169-409X(96)00494-2.

[5] E.A. Mueller, J.M. Kovarik, J.B. van Bree, W. Tetzloff, J. Grevel, K. Kutz, Improved Dose Linearity of Cyclosporine Pharmacokinetics from a Microemulsion Formulation, Pharm. Res. 11 (2) (1994) 301–304, https://doi.org/10.1023/A:1018923912135.

[6] C.W. Pouton, Formulation of self-emulsifying drug delivery systems, Adv. Drug Deliv. Rev. 25 (1) (1997) 47–58, https://doi.org/10.1016/S0169-409X(96)00490-5.

[7] N.H. Shah, M.T. Carvajal, C.I. Patel, M.H. Infeld, A.W. Malick, Self-emulsifying drug delivery systems (SEDDS) with polyglycolyzed glycerides for improving in vitro dissolution and oral absorption of lipophilic drugs, Int. J. Pharm. 106 (1) (1994) 15–23, https://doi.org/10.1016/0378-5173(94)90271-2.

[8] R. Neslihan Gursoy, S. Benita, Self-emulsifying drug delivery systems (SEDDS) for improved oral delivery of lipophilic drugs, Biomed. Pharmacother. 58 (3) (2004) 173–182, https://doi.org/10.1016/j.biopha.2004.02.001.

[9] P. Joyce, T.J. Dening, T.R. Meola, H.B. Schultz, R. Holm, N. Thomas, et al., Solidification to improve the biopharmaceutical performance of SEDDS: Opportunities and challenges, Adv. Drug Deliv. Rev. 142 (2019) 102–117, https://doi.org/10.1016/j.addr.2018.11.006.

[10] L.C. Alskär, C.J.H. Porter, C.A.S. Bergström, Tools for Early Prediction of Drug Loading in Lipid-Based Formulations, Mol. Pharm. 13 (1) (2016) 251–261, https://doi.org/10.1021/acs.molpharmaceut.5b00704.

[11] K. Rouaz, B. Chiclana-Rodríguez, A. Nardi-Ricart, M. Suñé-Pou, D. Mercadé-Frutos, J.M. Suñé-Negre, et al., Excipients in the Paediatric Population: A Review, Pharmaceutics. 13 (3) (2021) 387, https://doi.org/10.3390/pharmaceutics13030387.

[12] C. Albert, M. Beladjine, N. Tsapis, E. Fattal, F. Agnely, N. Huang, Pickering emulsions: Preparation processes, key parameters governing their properties and potential for pharmaceutical applications, J. Control. Release 309 (2019) 302–332, https://doi.org/10.1016/j.jconrel.2019.07.003.

[13] B.P. Binks, S.O. Lumsdon, Stability of oil-in-water emulsions stabilised by silica particles, PCCP 1 (12) (1999) 3007–3016, https://doi.org/10.1039/A902209K.

[14] B.P. Binks, Particles as surfactants—similarities and differences, Curr. Opin. Colloid Interface Sci. 7 (1-2) (2002) 21–41, https://doi.org/10.1016/S1359-0294(02)00008-0.

[15] L. Alison, P.A. Rühs, E. Tervoort, A. Teleki, M. Zanini, L. Isa, A.R. Studart, Pickering and Network Stabilization of Biocompatible Emulsions Using Chitosan-Modified Silica Nanoparticles, Langmuir 32 (50) (2016) 13446–13457, https://doi.org/10.1021/acs.langmuir.6b03439.

[16] K.M.Z. Hossain, L. Deeming, K.J. Edler, Recent progress in Pickering emulsions stabilised by bioderived particles, RSC Adv. 11 (62) (2021) 39027–39044, https://doi.org/10.1039/D1RA08086E.

[17] A. Sarkar, S. Zhang, M. Holmes, R. Ettelaie, Colloidal aspects of digestion of Pickering emulsions: Experiments and theoretical models of lipid digestion kinetics, Adv. Colloid Interface Sci. 263 (2019) 195–211, https://doi.org/10.1016/j.cis.2018.10.002.

[18] A. Awad, S.J. Trenfield, A. Goyanes, S. Gaisford, A.W. Basit, Reshaping drug development using 3D printing, Drug Discov. Today 23 (8) (2018) 1547–1555, https://doi.org/10.1016/j.drudis.2018.05.025.

[19] S.A. Khaled, J.C. Burley, M.R. Alexander, J. Yang, C.J. Roberts, 3D printing of five-in-one dose combination polypill with defined immediate and sustained release profiles, J. Control. Release 217 (2015) 308–314, https://doi.org/10.1016/j.jconrel.2015.09.028.

[20] S. Bom, R. Ribeiro, H.M. Ribeiro, C. Santos, J. Marto, On the progress of hydrogel-based 3D printing: Correlating rheological properties with printing behaviour, Int. J. Pharm. 615 (2022), https://doi.org/10.1016/j.ijpharm.2022.121506.

[21] Y. Cheng, H. Qin, N.C. Acevedo, X. Jiang, X. Shi, 3D printing of extended-release tablets of theophylline using hydroxypropyl methylcellulose (HPMC) hydrogels, Int. J. Pharm. 591 (2020), https://doi.org/10.1016/j.ijpharm.2020.119983.

[22] J. Rahman, J. Quodbach, Versatility on demand – The case for semi-solid micro-extrusion in pharmaceutics, Adv. Drug Deliv. Rev. 172 (2021) 104–126, https://doi.org/10.1016/j.addr.2021.02.013.

[23] I. El Aita, J. Rahman, J. Breitkreutz, J. Quodbach, 3D-Printing with precise layer-wise dose adjustments for paediatric use via pressure-assisted microsyringe printing, Eur. J. Pharm. Biopharm. 157 (2020) 59–65, https://doi.org/10.1016/j.ejpb.2020.09.012.

[24] A. Goyanes, C.M. Madla, A. Umerji, G. Duran Piñeiro, J.M. Giraldez Montero, M.J. Lamas Diaz, et al., Automated therapy preparation of isoleucine formulations using 3D printing for the treatment of MSUD: First single-centre, prospective, crossover study in patients, Int. J. Pharm. 567 (2019), https://doi.org/10.1016/j.ijpharm.2019.118497.

[25] I. Lafeber, J.M. Tichem, N. Ouwerkerk, A.D. van Unen, J.J.D. van Uitert, H.C.M. Bijleveld-Olierook, et al., 3D printed furosemide and sildenafil tablets: Innovative production and quality control, Int. J. Pharm. 603 (2021), https://doi.org/10.1016/j.ijpharm.2021.120694.

[26] N. Wang, H. Shi, S. Yang, 3D printed oral solid dosage form: Modified release and improved solubility, J. Control. Release 351 (2022) 407–431, https://doi.org/10.1016/j.jconrel.2022.09.023.

[27] M. Fanous, M. Bitar, S. Gold, A. Sobczuk, S. Hirsch, J. Ogorka, G. Imanidis, Development of immediate release 3D-printed dosage forms for a poorly water-soluble drug by fused deposition modeling: Study of morphology, solid state and dissolution, Int. J. Pharm. 599 (2021) 120417, https://doi.org/10.1016/j.ijpharm.2021.120417.

[28] S.J. Kim, J.C. Lee, J.Y. Ko, S.H. Lee, N.A. Kim, S.H. Jeong, 3D-printed tablets using a single-step hot-melt pneumatic process for poorly soluble drugs, Int. J. Pharm. 595 (2021), https://doi.org/10.1016/j.ijpharm.2021.120257.

[29] C.S. Katsiotis, M. Åhlén, M. Strømme, K. Welch, 3D-Printed Mesoporous Carrier System for Delivery of Poorly Soluble Drugs, Pharmaceutics. 13 (7) (2021) 1096, https://doi.org/10.3390/pharmaceutics13071096.

[30] P.P.D. Kondiah, T.A. Rants'o, S.S. Makhathini, S. Mdanda, Y.E. Choonara, An Oral 3D Printed PLGA-Tocopherol PEG Succinate Nanocomposite Hydrogel for High-Dose Methotrexate Delivery in Maintenance Chemotherapy, Biomedicines. 10 (7) (2022) 1470, https://doi.org/10.3390/biomedicines10071470.

[31] L. Lopez-Vidal, J.P. Real, D.A. Real, N. Camacho, M.J. Kogan, A.J. Paredes, et al., Nanocrystal-based 3D-printed tablets: Semi-solid extrusion using melting solidification printing process (MESO-PP) for oral administration of poorly soluble drugs, Int. J. Pharm. 611 (2022), https://doi.org/10.1016/j.ijpharm.2021.121311.

[32] B.W. Barber, C. Dumont, P. Caisse, G.P. Simon, B.J. Boyd, A 3D-Printed Polymer-Lipid-Hybrid Tablet towards the Development of Bespoke SMEDDS Formulations, Pharmaceutics. 13 (12) (2021) 2107, https://doi.org/10.3390/pharmaceutics13122107.

[33] K. Vithani, A. Goyanes, V. Jannin, A.W. Basit, S. Gaisford, B.J. Boyd, A Proof of Concept for 3D Printing of Solid Lipid-Based Formulations of Poorly Water-Soluble Drugs to Control Formulation Dispersion Kinetics, Pharm. Res. 36 (7) (2019) 102, https://doi.org/10.1007/s11095-019-2639-y.

[34] J. Johannesson, J. Khan, M. Hubert, A. Teleki, C.A.S. Bergström, 3D-printing of solid lipid tablets from emulsion gels, Int. J. Pharm. 597 (2021), https://doi.org/10.1016/j.ijpharm.2021.120304.

[35] C.W. Pouton, Formulation of poorly water-soluble drugs for oral administration: Physicochemical and physiological issues and the lipid formulation classification system, Eur. J. Pharm. Sci. 29 (3) (2006) 278–287, https://doi.org/10.1016/j.ejps.2006.04.016.

[36] H.D. Williams, P. Sassene, K. Kleberg, J.-C. Bakala-N'Goma, M. Calderone, V. Jannin, A. Igonin, A. Partheil, D. Marchaud, E. Jule, J. Vertommen, M. Maio, R. Blundell, H. Benameur, F. Carrière, A. Müllertz, C.J.H. Porter, C.W. Pouton, Toward the Establishment of Standardized In Vitro Tests for Lipid-Based Formulations, Part 1: Method Parameterization and Comparison of In Vitro Digestion Profiles Across a Range of Representative Formulations, J. Pharm. Sci. 101 (9) (2012) 3360–3380, https://doi.org/10.1002/jps.23205.

[37] V. De Graef, F. Depypere, M. Minnaert, K. Dewettinck, Chocolate yield stress as measured by oscillatory rheology, Food Res. Int. 44 (9) (2011) 2660–2665, https://doi.org/10.1016/j.foodres.2011.05.009.

[38] C. Tanger, M. Müller, D. Andlinger, U. Kulozik, Influence of pH and ionic strength on the thermal gelation behaviour of pea protein, Food Hydrocoll. 123 (2022), https://doi.org/10.1016/j.foodhyd.2021.106903.

[39] D. Zhang, T. Mu, H. Sun, Calorimetric, rheological, and structural properties of potato protein and potato starch composites and gels, Starch - Stärke 69 (7–8) (2017) 1600329, https://doi.org/10.1002/star.201600329.

[40] B.P. Binks, C.P. Whitby, Nanoparticle silica-stabilised oil-in-water emulsions: improving emulsion stability, Colloids Surf Physicochem Eng Asp. 253 (1) (2005) 105–115, https://doi.org/10.1016/j.colsurfa.2004.10.116.

[41] M. Kargar, K. Fayazmanesh, M. Alavi, F. Spyropoulos, I.T. Norton, Investigation into the potential ability of Pickering emulsions (food-grade particles) to enhance the oxidative stability of oil-in-water emulsions, J. Colloid Interface Sci. 366 (1) (2012) 209–215, https://doi.org/10.1016/j.jcis.2011.09.073.

[42] P. Finkle, H.D. Draper, J.H. Hildebrand, The theory of emulsification, J. Am. Chem. Soc. 45 (12) (1923) 2780–2788, https://doi.org/10.1021/ja01665a002.

[43] J. Gao, X. Bu, S. Zhou, X. Wang, M. Bilal, F.U. Hassan, et al., Pickering emulsion prepared by nano-silica particles – A comparative study for exploring the effect of various mechanical methods, Ultrason. Sonochem. 83 (2022), https://doi.org/10.1016/j.ultsonch.2022.105928.

[44] T. Bollhorst, T. Grieb, A. Rosenauer, G. Fuller, M. Maas, K. Rezwan, Synthesis Route for the Self-Assembly of Submicrometer-Sized Colloidosomes with Tailorable Nanopores, Chem. Mater. 25 (17) (2013) 3464–3471, https://doi.org/10.1021/cm401610a.

[45] I. Akartuna, A.R. Studart, E. Tervoort, U.T. Gonzenbach, L.J. Gauckler, Stabilization of Oil-in-Water Emulsions by Colloidal Particles Modified with Short

Amphiphiles, Langmuir 24 (14) (2008) 7161–7168, https://doi.org/10.1021/la800478g.

[46] B.P. Binks, A. Desforges, D.G. Duff, Synergistic Stabilization of Emulsions by a Mixture of Surface-Active Nanoparticles and Surfactant, Langmuir 23 (3) (2007) 1098–1106, https://doi.org/10.1021/la062510y.

[47] L. Ridel, M.A. Bolzinger, N. Gilon-Delepine, P.Y. Dugas, Y. Chevalier, Pickering emulsions stabilized by charged nanoparticles, Soft Matter 12 (36) (2016) 7564–7576, https://doi.org/10.1039/C6SM01465H.

[48] T.S. Horozov, B.P. Binks, Particle-Stabilized Emulsions: A Bilayer or a Bridging Monolayer? Angew. Chem. Int. Ed. 45 (5) (2006) 773–776, https://doi.org/10.1002/anie.200503131.

[49] P. Sufi-Maragheh, N. Nikfarjam, Y. Deng, N. Taheri-Qazvini, Pickering emulsion stabilized by amphiphilic pH-sensitive starch nanoparticles as therapeutic containers, Colloids Surf. B Biointerfaces 181 (2019) 244–251, https://doi.org/10.1016/j.colsurfb.2019.05.046.

[50] J. Frelichowska, M.A. Bolzinger, Y. Chevalier, Effects of solid particle content on properties of o/w Pickering emulsions, J. Colloid Interface Sci. 351 (2) (2010) 348–356, https://doi.org/10.1016/j.jcis.2010.08.019.

[51] J.S. Patton, M.C. Carey, Watching Fat Digestion, Science 204 (4389) (1979) 145–148, https://doi.org/10.1126/science.432636.

[52] F.S. Nielsen, K.B. Petersen, A. Müllertz, Bioavailability of probucol from lipid and surfactant based formulations in minipigs: Influence of droplet size and dietary state, Eur. J. Pharm. Biopharm. 69 (2) (2008) 553–562, https://doi.org/10.1016/j.ejpb.2007.12.020.

[53] A.-C. Jacobsen, A. Kabedev, P.D. Sinko, J.E. Palm, C.A.S. Bergström, A. Teleki, Intrinsic lipolysis rate for systematic design of lipid-based formulations. Drug Deliv, Transl. Res. 13 (5) (2023) 1288–1304, https://doi.org/10.1007/s13346-022-01246-y.

[54] P.E. Ruiz-Rodriguez, D. Meshulam, U. Lesmes, Characterization of Pickering O/W Emulsions Stabilized by Silica Nanoparticles and Their Responsiveness to In vitro Digestion Conditions, Food Biophys. 9 (4) (2014) 406–415, https://doi.org/10.1007/s11483-014-9346-3.

[55] R.V. Tikekar, Y. Pan, N. Nitin, Fate of curcumin encapsulated in silica nanoparticle stabilized Pickering emulsion during storage and simulated digestion, Food Res. Int. 51 (1) (2013) 370–377, https://doi.org/10.1016/j.foodres.2012.12.027.

[56] X. Lu, Q. Huang, Stability and in vitro digestion study of curcumin-encapsulated in different milled cellulose particle stabilized Pickering emulsions, Food Funct. 11 (1) (2020) 606–616, https://doi.org/10.1039/C9FO02029B.

[57] H.D. Williams, P. Sassene, K. Kleberg, M. Calderone, A. Igonin, E. Jule, J. Vertommen, R. Blundell, H. Benameur, A. Müllertz, C.W. Pouton, C.J.H. Porter, Toward the Establishment of Standardized In Vitro Tests for Lipid-Based Formulations, Part 3: Understanding Supersaturation Versus Precipitation

[58] Potential During the In Vitro Digestion of Type I, II, IIIA, IIIB and IV Lipid-Based Formulations, Pharm. Res. 30 (12) (2013) 3059–3076, https://doi.org/10.1007/s11095-013-1038-z.

[58] A.M. Kaukonen, B.J. Boyd, C.J.H. Porter, W.N. Charman, Drug Solubilization Behavior During in Vitro Digestion of Simple Triglyceride Lipid Solution Formulations, Pharm. Res. 21 (2) (2004) 245–253, https://doi.org/10.1023/B:PHAM.0000016282.77887.1f.

[59] P.J. Sassene, M.H. Michaelsen, M.D. Mosgaard, M.K. Jensen, E. Van Den Broek, K. M. Wasan, H. Mu, T. Rades, A. Müllertz, In Vivo Precipitation of Poorly Soluble Drugs from Lipid-Based Drug Delivery Systems, Mol. Pharm. 13 (10) (2016) 3417–3426, https://doi.org/10.1021/acs.molpharmaceut.6b00413.

[60] N. Thomas, K. Richter, T.B. Pedersen, R. Holm, A. Müllertz, T. Rades, In Vitro Lipolysis Data Does Not Adequately Predict the In Vivo Performance of Lipid-Based Drug Delivery Systems Containing Fenofibrate, AAPS J. 16 (3) (2014) 539–549, https://doi.org/10.1208/s12248-014-9589-4.

[61] B.T. Griffin, M. Kuentz, M. Vertzoni, E.S. Kostewicz, Y. Fei, W. Faisal, C. Stillhart, C.M. O'Driscoll, C. Reppas, J.B. Dressman, Comparison of in vitro tests at various levels of complexity for the prediction of in vivo performance of lipid-based formulations: case studies with fenofibrate, Eur. J. Pharm. Biopharm. 86 (3) (2014) 427–437, https://doi.org/10.1016/j.ejpb.2013.10.016.

[62] Y. Cheng, H. Qin, N.C. Acevedo, X. Shi, Development of methylcellulose-based sustained-release dosage by semisolid extrusion additive manufacturing in drug delivery system, J Biomed Mater Res - Part B Appl Biomater. 109 (2) (2021) 257–268, https://doi.org/10.1002/jbm.b.34697.

[63] P. Polamaplly, Y. Cheng, X. Shi, K. Manikandan, X. Zhang, G.E. Kremer, et al., 3D printing and characterization of hydroxypropyl methylcellulose and methylcellulose for biodegradable support structures, Polymer 173 (2019) 119–126, https://doi.org/10.1016/j.polymer.2019.04.013.

[64] M. Lille, A. Nurmela, E. Nordlund, S. Metsä-Kortelainen, N. Sozer, Applicability of protein and fiber-rich food materials in extrusion-based 3D printing, J. Food Eng. 220 (2018) 20–27, https://doi.org/10.1016/j.jfoodeng.2017.04.034.

[65] M.R. Sommer, L. Alison, C. Minas, E. Tervoort, P.A. Rühs, A.R. Studart, 3D printing of concentrated emulsions into multiphase biocompatible soft materials, Soft Matter 13 (9) (2017) 1794–1803, https://doi.org/10.1039/C6SM02682F.

[66] A.T. Chatzitaki, E. Mystiridou, N. Bouropoulos, C. Ritzoulis, C. Karavasili, D. G. Fatouros, Semi-solid extrusion 3D printing of starch-based soft dosage forms for the treatment of paediatric latent tuberculosis infection, J. Pharm. Pharmacol. 74 (10) (2022) 1498–1506, https://doi.org/10.1093/jpp/rgab121.

[67] S.A. Khaled, J.C. Burley, M.R. Alexander, C.J. Roberts, Desktop 3D printing of controlled release pharmaceutical bilayer tablets, Int. J. Pharm. 461 (1) (2014) 105–111, https://doi.org/10.1016/j.ijpharm.2013.11.021.